

Massless Dirac fermions in stable two-dimensional carbon-arsenic monolayerC. Kamal *Theory and Simulations Laboratory, HRDS, Raja Ramanna Centre for Advanced Technology, Indore - 452013, India and Homi Bhabha National Institute, Training School Complex, Anushakti Nagar, Mumbai-400094, India*

(Received 3 April 2019; revised manuscript received 1 September 2019; published 5 November 2019)

We predict from density functional theory based electronic structure calculations that a monolayer made up of carbon and arsenic atoms with a chemical composition (CAs_3) forms an energetically and dynamically stable system in two geometrical arrangements, namely, buckled and puckered configurations. The results of electronic structure calculations predict that the puckered monolayer is a metal, whereas the buckled monolayer is a semimetal. Interestingly, the electronic band structure of the buckled configuration possesses a linear dispersion and a Dirac cone at the Fermi level around the high-symmetry K point in the reciprocal lattice. Thus, at low-energy excitation (up to 105 meV), the charge carriers in this system behave as massless Dirac fermions. Detailed analysis of partial density of state indicates that the $2p_z$ orbital of C atoms contributes significantly to the states which form the linear dispersion and hence the Dirac cone around the Fermi level. This suggests the existence of a strong correlation between the linear dispersion (Dirac cone) and sp^2 -like hybridization of the orbitals of C atom. Thus the electronic properties of CAs_3 monolayer are similar to those of graphene and other group-IV based monolayers like, silicene and germanene. In addition, we have also investigated the influence of mechanical strain on the properties of CAs_3 monolayer. Our results indicate that the monolayer possesses linear dispersion in the electronic band structure for a wide range of mechanical strain from -12% to 20% , though the position of Dirac point may not lie exactly at the Fermi level. Finally, we wish to point out that CAs_3 monolayer belongs to the class of *Dirac materials* where the behavior of particles, at low-energy excitations, is characterized by the Dirac-like Hamiltonian rather than the Schrodinger Hamiltonian.

DOI: [10.1103/PhysRevB.100.205404](https://doi.org/10.1103/PhysRevB.100.205404)**I. INTRODUCTION**

Research on two-dimensional (2D) materials has increased tremendously after the discovery of graphene—an atom-thin honeycomb monolayer of carbon. Graphene is considered a *wonder material* because it possesses many novel properties such as the charge carriers in this material behave as Dirac fermion, Klein tunneling, anomalous half-integer quantum Hall effect, finite dc conductivity, etc. [1,2]. Researchers around the world have been searching for new graphene-like 2D materials made up of different elements, in particular, from the p block of the periodic table. There has been significant progress in this direction. In the last decade, several new 2D monolayers have been theoretically predicted to be stable [3–24] and later quite a few of them have been successfully grown experimentally [25–41]. In analogy with graphene, the 2D monolayers based on p -block elements (given in parenthesis) are named as borophene (B), aluminene (Al), silicene (Si), germanene (Ge), stanene (Sn), plumbene (Pb), phosphorene (P), arsenene (As), antimonene (Sb), bismuthene (Bi), etc. From the numerous studies available in the literature, many interesting properties of the above mentioned 2D materials have been revealed. Some of the important outcomes from these studies [3–41], which are relevant to the present paper, are given below.

Similar to graphene, the group IV based monolayers such as silicene, germanene, and stanene are found to be semimetal and all of them possess a Dirac cone at the Fermi level (E_F) around the high-symmetry K point in the reciprocal lattice.

Hence the charge carriers in these monolayers behave as massless Dirac fermion at their low-energy excitation. It is important to note that these group IV based monolayers stabilize in a buckled geometric configuration which is different from the planar geometry of graphene. However, the buckling in the geometry does not alter the presence of Dirac cone at the E_F . It has been reported in the literature that the buckling will play an important role in inducing a band gap when the monolayers are subjected to external transverse electric field [11,42–45]. It is well known that many properties of materials are determined by the nature of states around the Fermi level. In case of the group IV based 2D materials, the properties of materials at low-energy excitation are characterized by the Dirac fermion (the linear dispersion around the E_F) unlike the usual Schrodinger-Fermion (parabolic-like dispersion). Due to this reason, the group IV based 2D monolayers, including graphene, belong to a class of material called *Dirac materials* [46] in which the low-energy excited carriers follow the Dirac-like Hamiltonian. Until now, many different materials have been shown to possess particles which behave as Dirac fermion and consequently many of their properties at the low-energy excitations are universal [46].

On the other hand, the studies on the properties of group III based 2D materials such as aluminene and borophene show that these are metals whereas the group V monolayers (phosphorene, arsenene, antimonene, and bismuthene) behave as semiconductors. The electronic band structure calculations of free standing borophene show that it is a highly anisotropic metal due to crossing of bands along Γ -X and S-Y directions

[25]. In case of aluminene, the electronic band structure resemble very close to that of graphene, but the Dirac cone lies well above the E_F (by the amount 1.618 eV) [6]. This is due to fact that Al atom is trivalent as compared to tetravalency of C atom and hence the p_z orbital is not completely filled. It is clearly observed that the monolayer has a finite DOS at the Fermi level and hence shows interesting Fermi curves [6]. In contrast, phosphorene is a direct band semiconductor and it has very high hole mobility [19]. In addition, a band gap can be tuned by varying the number of layers [19]. Hence, these results are considered to be important from the applications point of view. Few devices based on phosphorene have also been demonstrated [37]. Another group V based monolayer namely arsenene is found to be indirect band gap semiconductor, but namely it goes from indirect to direct due to applications of very small amount of mechanical strain [22]. Thus this can also be a potential candidate for many optoelectronic applications. Moreover, semiconducting behavior is also observed in case of antimonene and bismuthene monolayers [23,24]. Apart from the elemental monolayers, investigations on the properties of binary monolayers have also been reported in the literature. Sahin *et al.* have carried out detailed investigation on several properties of group III-V based binary monolayers which are all found to be semiconducting in nature [47]. Similarly, computational study on the electronic properties of group IV-VI based monolayer reveals that they are also semiconductors [48]. In contrast to metallic character of GeP_3 and SnP_3 bulk systems, the monolayer counterparts of these two group IV-V based systems are found to be semiconductors [49–51]

We note here that all the binary monolayers made up of p -block elements as well as the elemental monolayers of group III and V elements reported in the literature are either semiconductor or metal. Thus they do not exhibit properties similar to those of graphene and other group IV based monolayers which are all semimetal and possess Dirac cone at the E_F . Since the Dirac materials show many exciting properties, it is important to explore the possibility of discovering different types of new graphenelike 2D monolayers which may possess massless Dirac fermions. This will be expected to widen the scope of the research in 2D materials because many of these materials are considered as potential candidates for several technological applications, in particular, in the field of flexible electronics due to their excellent electronic properties [52]. Thus searching for new 2D Dirac materials is very important from both the fundamental as well as application points of view.

With the above mentioned motivations, we explore the possibility of finding a stable binary monolayer made up of group IV and V elements, namely, C and As atoms, respectively. It may be worth probing the stability and properties of monolayers with other possible combinations of group IV and V elements as well. In the present work, we choose to study the stability and various physical properties such as geometric, electronic, and vibrational properties of carbon-arsenic (CAs_3) monolayer, in three geometrical arrangements, namely, planar, buckled, and puckered configurations by employing density functional theory (DFT) based electronic structure calculations. Results of our phonon and cohesive energy calculations show that CAs_3 monolayer in buckled and

puckered configurations is both energetically and dynamically stable. Planar CAs_3 monolayer is found to be unstable. The results of electronic band structure suggest that puckered configuration is a metal. On the other hand, like graphene, buckled CAs_3 monolayer is found to be a semimetal and possesses a linear dispersion and a Dirac cone at the E_F around the high-symmetry K point in the reciprocal lattice. Thus the charge carriers in this material behave as massless Dirac fermion. The energy range through which the Dirac cone exists is from nearly -600 to 250 meV. However, due to the presence of a parabolic-like dispersion curve at Γ point around 105 meV above the E_F , the characteristic of Dirac fermion like behavior of electronlike particle is limited to excitation up to 105 meV. For excitation beyond this energy, the contributions from Schrodinger-like particles will also be included. In addition, we have also studied the influence of mechanical strain on the geometric and electronic properties of the CAs_3 monolayer. Our results suggest that there is a transition from the buckled to a planar configuration when an applied tensile strain goes beyond 18% . For a wide range of mechanical strains (-12% to 20%), the monolayer possesses the linear dispersion, though the position of the Dirac point does not lie exactly at the E_F . Detailed analysis indicates that the drastic changes in the geometrical environment around C atom for a compressive strain beyond -12% cause the linear dispersion to disappear.

The paper has been organized in the following manner. Next section contains the details of computational approach employed in the present study. It is then followed by results and discussion in Sec. III. Finally, we conclude our results in the last section.

II. COMPUTATIONAL DETAILS

We employ Vienna *ab initio* simulation package (VASP) [53] within the framework of the projector augmented wave (PAW) [54] method to perform density functional theory (DFT) [55] based electronic structure calculations. For an exchange-correlation (XC) functional, we choose generalized gradient approximation (GGA) given by Perdew, Burke, and Ernzerhof (PBE) [56]. The plane waves are expanded with the energy cutoff of 400 eV. We use Γ -centered k mesh of $31 \times 31 \times 1$ and $21 \times 15 \times 1$ for planar/buckled and puckered configurations, respectively, for Brillouin zone integrations. The convergence criterion for energy in SCF cycle is chosen to be 10^{-6} eV. The geometric structure is optimized by minimizing the forces on individual atoms with the criterion that the total force on each atom is below 10^{-2} eV/Å. A vacuum of about 18 Å is applied in the direction perpendicular to the plane of 2D sheet to make the interaction between two adjacent unit cells in the periodic arrangement is negligible. Drawing of geometry and charge density has been done using VESTA software [57]. For phonon calculations, we use small displacement method as implemented in PHONOPY code [58]. In order to calculate force constant, few atoms have been displaced in a supercell $3 \times 3 \times 1$ and $2 \times 2 \times 1$ respectively for planar/buckled and puckered configurations. For the chemical bonding analysis based on crystal orbital Hamilton population (COHP), we use the local orbital basis

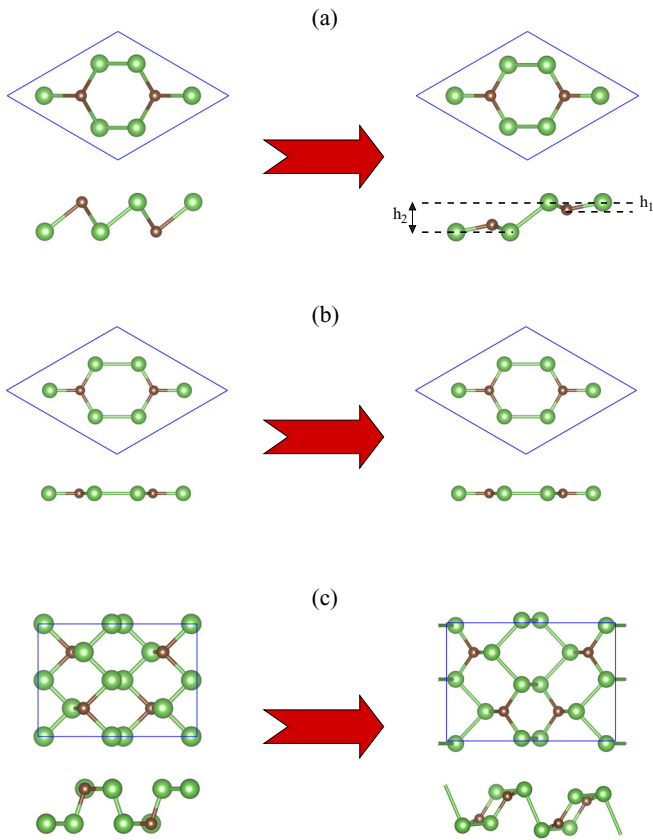


FIG. 1. Top and side views of initial and optimized geometric structures of CAs_3 monolayer in (a) buckled, (b) planar, and (c) puckered configurations. The vertical distances h_1 and h_2 represent the buckling lengths in the optimized geometry of the buckled configuration. Small and big balls depict carbon and arsenic atoms respectively.

suite towards electronic-structure reconstruction (LOBSTER) [59] program.

III. RESULTS AND DISCUSSION

A. Geometric structure and stability

Figure 1 shows the initial and optimized geometric structures of CAs_3 monolayer in three different geometric arrangements, namely, (a) buckled, (b) planar, and (c) puckered configurations. These initial geometries are similar to those of silicene, graphene, and phosphorene in $2 \times 2 \times 1$ supercell, respectively. The unit cell of CAs_3 monolayer in planar and buckled configurations contains two carbon and six arsenic atoms. The puckered configuration contains four carbon and 12 arsenic atoms in an unit cell. Results of the optimized geometrical parameters (lattice constant, bond lengths, and bond angles) and binding energies for these three configurations are summarized in Table I. We have observed that the planar configuration retains its geometry, whereas the buckled structure is converged to a slightly different geometry. The value of lattice constant for buckled geometry is found to be 6.778 Å, which is much shorter than that (7.964 Å) of planar configuration. In case of puckered configuration, the calculated lattice constants are 6.797 and 9.658 Å for

TABLE I. The results for the binding energy, lattice constant, bond length, and bond angle of CAs_3 monolayer obtained from DFT based calculations with GGA XC functional.

Geometry	Binding energy E_B (eV/atom)	Lattice constant a_0 (b_0) (Å)	Bond length (Å)	Bond angle (°)
buckled	-3.584	6.778	1.920 (As-C)	116.09 (As-C-As)
			2.565 (As-As)	86.64 (As-As-As)
				105.41 (C-As-As)
planar	-3.258	7.964	1.897 (As-C)	120 (As-As-As)
			2.701 (As-As)	120 (C-As-As)
puckered	-3.569	6.797 9.658	1.930, 1.905 (As-C)	118.10, 108.95 (As-C-As)
			2.685, 2.518 (As-As)	94.43, 102.36 (As-As-As)
				114.21, 102.71, 90.79 (C-As-As)

a and b directions, respectively. Neighboring atoms in the initial geometry of the buckled configuration (as well as in silicene-like geometry) lie in two different planes and the vertical distance between the atoms in these two planes is called buckling length. However, in the optimized geometry of CAs_3 monolayer, C and As atoms have moved to two different sets of planes and thus overall two buckling distances, namely, h_1 and h_2 are required to characterize the buckling in the system: the former is the vertical distance between a C atom and its neighboring As atom and the latter is the vertical distance between two neighboring As atoms. It is to be noted that when h_1 and h_2 become zero, the buckled structure will reduce to planar structure. Our calculated values of As-C and As-As bond lengths for buckled configuration are 1.920 and 2.565 Å, respectively. However, reduction of As-C bond (1.897 Å) and extension of As-As bond (2.701 Å) have been observed for the planar configuration. In case of the puckered configuration, the optimized geometry contains two sets of As-C and As-As bond lengths and they are 1.930, 1.905 Å and 2.685, 2.518 Å, respectively. The characteristic bond angle of 120° between the constituent atoms is retained in honeycomb lattice of planar configuration. In case of the buckled configuration, three different types of bond angles, namely As-C-As (116.09°), As-As-As (86.64°), and C-As-As (105.41°) have been observed. We wish to note here that the bond angles centered around As atoms are much smaller as compared to those around C atoms. Though the bonding arrangement around As atoms seems similar to that of NH_3 molecule, the bond angles deviate strongly from that of sp^3 hybridization. However, we find that C atoms prefer to be in sp^2 -like hybridization. A buckling distance (h_1) between C and As atoms is found to be 0.385 Å. Further, the lower value of bond angle between As atoms and the higher value of buckling length ($h_2 = 1.565$ Å) as compared to those observed in buckled arsenene (92.22° , 1.388 Å) [22] clearly indicate that the effect of buckling is stronger in CAs_3 monolayer rather than that in buckled arsenene. On the other hand, puckered CAs_3 monolayer possesses more than one value of bond angles for the above mentioned three bond angles and

values are summarized in Table I. The different values of bond angles around C and As atoms suggest presence of strong anisotropic bonding arrangement in the puckered lattice.

In order to check the stability of CAS_3 monolayer, we have calculated the binding energy (per atom) of the system in the planar, buckled and puckered configurations by using the expression

$$E_B = (E_{\text{CAS}_3} - n_C E_C - n_{\text{As}} E_{\text{As}}) / (n_C + n_{\text{As}}), \quad (1)$$

where E_{CAS_3} , E_C , and E_{As} represent the energies of CAS_3 monolayer and carbon and arsenic atoms, respectively. n_C and n_{As} are the number of carbon and arsenic atoms in the unit cell, respectively. We find that CAS_3 monolayer in all three configurations forms a bound system since the binding energies are negative in all the three configurations. Among these three configurations, the buckled monolayer is found to be the minimum energy configuration. The binding energy per atom of the buckled configuration is -3.584 eV/atom and the puckered configuration is 15 meV/atom above this value. However, the planar configuration is 326 meV/atom energetically higher than that of the buckled configuration. This is possibly due to the fact that the arsenic atom, being pentavalent, prefers sp^3 hybridization rather than sp^2 . Comparison of binding energy of CAS_3 monolayer with those of group V and IV monolayers suggests that it is energetically more favorable as compared to those of phosphorene (~ -3.425 eV/atom) [60], arsenene (-2.989 eV/atom) [22], antimonene (-2.87 eV/atom) [61], and germanene (-3.39 eV/atom) [62], but it is less favorable when it is compared with silicene (-3.903 eV/atom) [10]. It is also more favorable as compared many group IV-VI based binary monoalyers such as SnS , SiSe , GeSe , SnSe , SiTe , GeTe , and SnTe [48].

In addition to the binding energy calculations, we have carried out phonon calculations for buckled, planar and puckered configurations to check the dynamical stability of CAS_3 monolayer. The plots for the phonon dispersions and density of states are given in Fig. 2. The results of phonon dispersions suggest that the both buckled and puckered structures are dynamically stable since the frequencies of all the modes are positive, except a negligible negative frequency in transverse acoustic mode close to Γ point, for the puckered configuration. However, in case of the planar configuration, we find that many of the modes possess imaginary frequencies (shown as negative frequencies) throughout the Brillouin zone and hence the planar structure will not be dynamically stable, though it has negative binding energy. Thus we shall concentrate now on the properties of the buckled and puckered structures and not those of dynamically unstable planar configuration. From Fig. 2(a), we observe that the phonon dispersion curves of buckled structure contain three acoustic modes in which two are longitudinal and one is transverse. Around Γ point, the dispersion curves of the longitudinal modes vary in linear fashion whereas the transverse acoustic (ZA) mode shows a parabolic dispersion. The parabolic-like variation in transverse acoustic mode is the characteristic of a two-dimensional system and similar variation is observed for graphene, silicene, germanene, arsenene, etc. [7,15,19,22].

Phonon density of states (DOS) of the buckled configuration contains four regions of vibrational energy bands (three optical and one acoustic) and three gaps exist between them

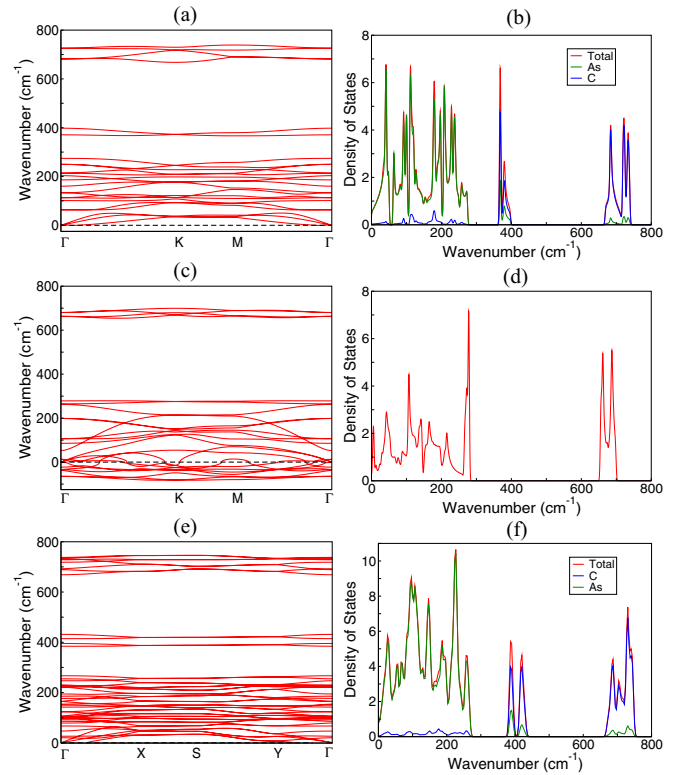


FIG. 2. The phonon dispersion curves along the high-symmetry k points in Brillouin zone and density of states for CAS_3 monolayer in the buckled [(a) and (b)], planar [(c) and (d)], and puckered [(e) and (f)] configurations.

[see Fig. 2(b)]. The smallest energy gap of 13 cm^{-1} is observed between acoustic and first optical band. In case of the puckered configuration, the bands of acoustic and first optical modes overlap each other. Thus there are only three regions of bands in this case. Detailed analysis of partial DOS for these two configuration indicates that the major contribution for the acoustic and first optical bands is due to the vibration of As atoms. The narrow band which occurs around 400 cm^{-1} has contributions from both C and As atoms. On the other hand, the states with higher vibrational energy (above 650 cm^{-1}) have contribution mainly due to carbon atoms.

B. Electronic band structure

In this section, we shall discuss the electronic properties of CAS_3 monolayer in the buckled and puckered configurations. The results for the electronic band structures and DOS are given in Figs. 3 and 4, respectively. The results of our calculations indicate that the buckled monolayer is a semimetal as the value of DOS at the E_F is zero where as the puckered monolayer is found to be metal since it has a finite value of DOS at the Fermi level. We observe that there are few bands with parabolic dispersion around the Fermi level in puckered configuration. The crossing of the bands has been observed along $Y-\Gamma$, $\Gamma-X$, and $S-\Gamma$ directions which provide conduction channels for this configuration.

Most important observation from the present calculations is that the electronic band structure of CAS_3 monolayer in

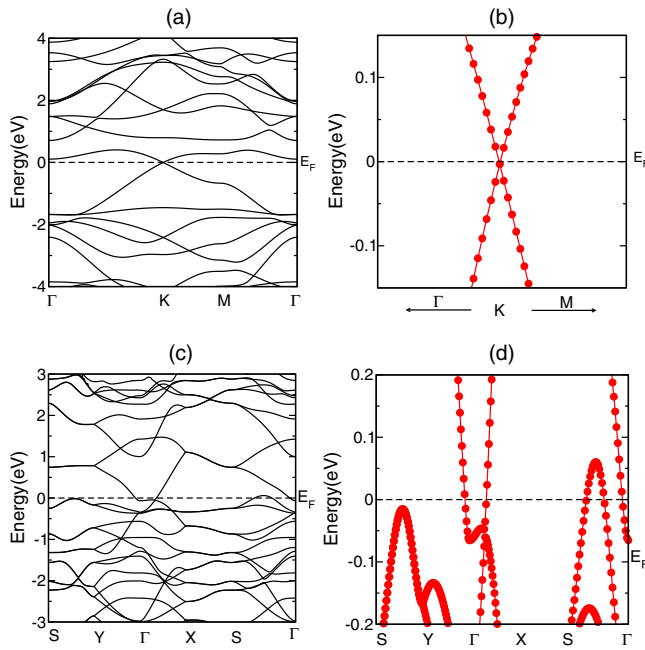


FIG. 3. The electronic band structure of CAS_3 in the buckled [(a) and (b)] and puckered [(c) and (d)] configurations along the high-symmetry k points in two different energy ranges.

buckled configuration contains linear dispersion around the E_F at the high-symmetry K point. Thus the carriers in the states close to the E_F behave as massless Dirac fermions. These results suggest that the electronic properties of CAS_3 monolayer in this respect is similar to those of graphene and other group IV monolayers. The range of linear dispersion in the valence and conduction bands is from -600 to 250 meV. We have estimated the Fermi velocity of charge carriers. The calculated value is 3.49×10^5 m/s which is less than that of graphene (with range $0.85\text{--}3 \times 10^6$), but comparable with those found in silicene (5.27×10^5 m/s) and germanene (5.09×10^5 m/s) [63]. In Fig. 5, we have also drawn the three-dimensional (3D) plots for (a) highest occupied conduction and (b) lowest unoccupied valence bands in their full energy range. The subfigures (c) and (d) show the combined bands in two different energy ranges. The top and bottom of xy plane also contain contour plots of the bands. We can clearly see the presence of Dirac cones in the 3D plot of energy versus (k_x, k_y) . There exist six Dirac cones at the edges of the hexagons (high-symmetry K point) around the E_F . The presence of paraboloid-like band with minima at Γ point is also visible in sub-figures (a) and (d). The bottom of the paraboloid is at 105 meV above the E_F . Due to this, the range of observing purely Dirac fermion like behavior of particle (electronlike) will be restricted from 0 to 105 meV. For any excitations with energy above 105 meV, we shall observe a mixed behavior due to the presence of both Dirac and Schrodinger like fermions. We would like to mention here that the energy of 105 meV is much higher than the thermal energy $k_B T$ at the room temperature. Thus most of the charge carriers in this material are expected to behave as Dirac fermions at the room temperature. Similar to graphene, it may be possible to tune the position of the E_F from 105 to -600 meV by appropriate gate voltage and

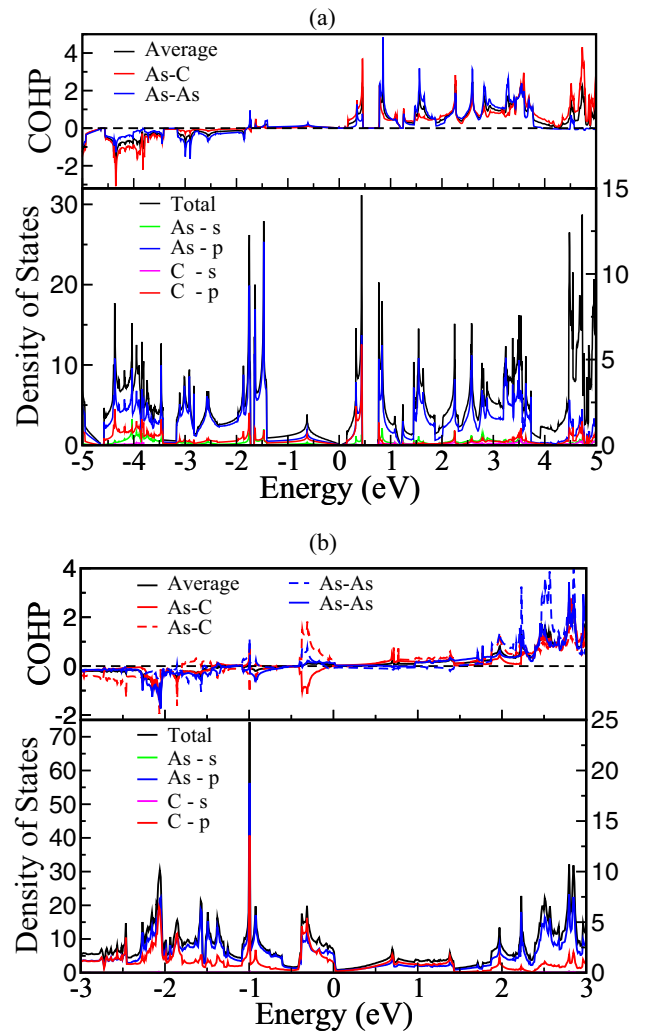


FIG. 4. Total (DOS) and partial (PDOS) electronic density of states for CAS_3 monolayer in (a) buckled and (b) puckered configurations. The COHP analysis of As-C and As-As bonds have also been included in the plots.

thus, increase or decrease the value of conductivity of Dirac fermion. Furthermore, the polarity of the carriers (electron- or holelike) will be decided by the position of the E_F . It may also be possible to tune the E_F by external influences like, electron or hole doping, strain, etc. We shall discuss the effect of mechanical strain on the properties of CAS_3 monolayer in the next section.

In order to understand the nature of states specially around the E_F , we have also carried out detailed analysis of the partial electronic DOS for both buckled and puckered configurations (see Fig. 4). In addition, we have calculated crystal orbital Hamilton population (COHP) for these two configurations and results are included (above the DOS plots) in Fig. 4. Our analysis suggests that both the valence and conduction bands (Fig. 4) have contributions from s and p orbitals of both the constituent atoms. It clearly indicates the presence of strong hybridization between the orbitals of As and C atoms. By analyzing further, we find that the contributions from $3p$ orbitals of As atom is predominant in the range of energies presented in Fig. 4, except for the states close to the E_F . This is due to

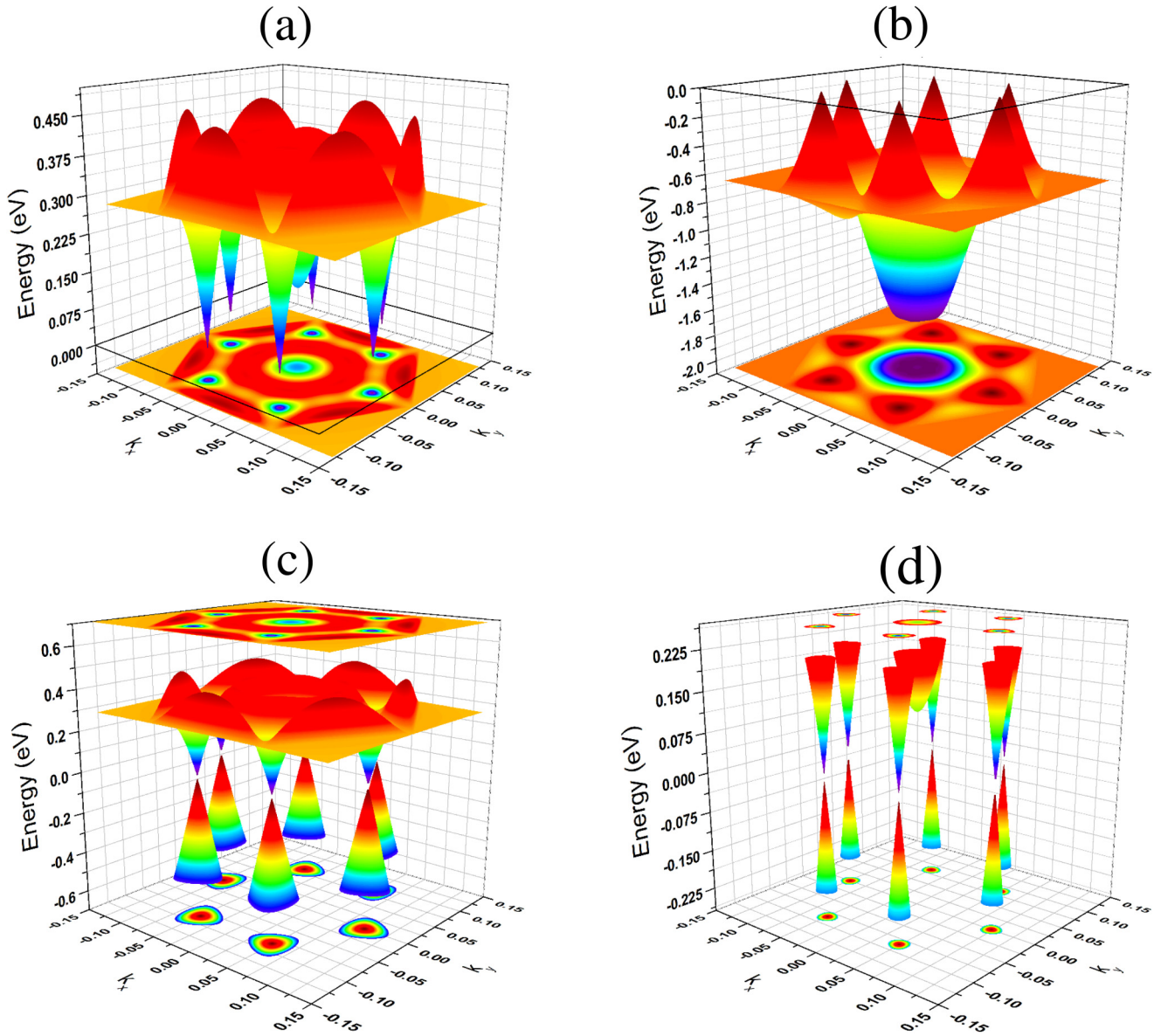


FIG. 5. Three-dimensional (3D) plots of electronic band structure of CA_3 monolayer in buckled configuration: (a) lowest unoccupied conduction and (b) highest occupied valence bands which are close to the Fermi level. Combined plots of these two bands are given (c) and (d) in two different energy ranges. Presence of Dirac cones at the Fermi level is clearly visible in (d).

fact that the unit cell contains more number of As atoms which have more number of electrons in $3p$ orbitals as compared to C atoms ($2p$ orbitals). In buckled configuration, for states around the E_F (from -1.5 to 0.5 eV), it is clearly visible from partial DOS that the amount of contribution of $2p$ orbitals of C atom is at par with that of $3p$ orbitals of As atoms. As mentioned above the number of C atoms in the unit cell is two as compared to six As atom. Thus, if we scale the partial DOS of C and As atom by their numbers in the unit cell (two and six, respectively), the states close to the E_F have more $2p$ orbital (of C atom) character as compared to $3p$ orbital of As atom.

The results of COHP analysis indicate that the valence and conduction bands in buckled configuration are mostly due to bonding (value of COHP < 0) and antibonding (value of COHP > 0) character, respectively. This suggests that the buckled configuration is electronically stable since most of

bonding (antibonding) orbitals are occupied (unoccupied). We also find that contributions from As-C and As-As bonds are nearly same for the energy ranges given in Fig. 4. On the other hand, for puckered configuration, there are significant contributions from the anti-bonding character in valence bands near the Fermi level. Detailed analysis of bond weighted COHP shows that the antibonding character of states just below the Fermi level arise due to the longer bond lengths namely 1.930 Å (As-C) and 2.685 Å (As-As). It is to be noted here that there are more than one type of bond lengths for both As-C and As-As in case of the puckered configuration.

It will be interesting to compare the properties of CA_3 monolayer in the buckled configuration with those of buckled arsenene, because the former can be thought as carbon substituted arsenene. In buckled arsenene monolayer, As atom, with five valence electrons, favors sp^3 -like hybridization

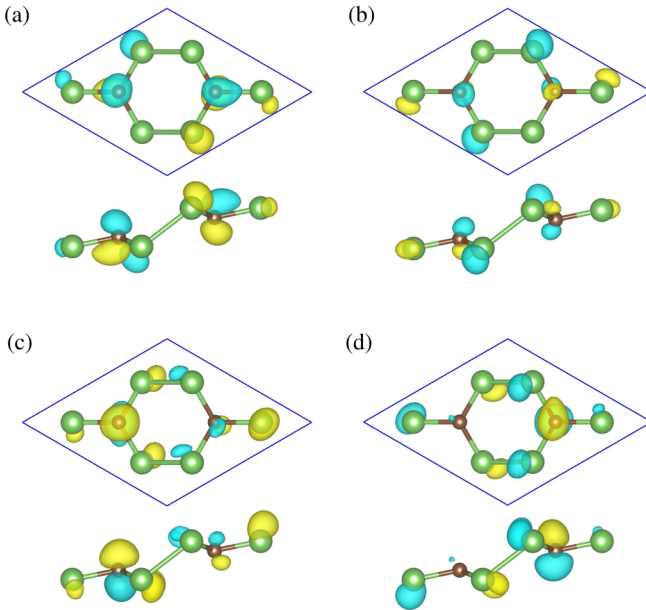


FIG. 6. The spatial distributions of Kohn-Sham states at Dirac point which lies at the high-symmetry K point and the E_F . Real and imaginary parts of the occupied [(a) and (b)] and unoccupied [(c) and (d)] orbitals.

which leads to semiconducting character of the system. On the other hand, Carbon atoms present in CAs_3 monolayer makes the geometrical arrangement different from those of As in arsenene. For example, the results of geometric structure for the buckled configuration show that the bond angles around C atom is 116.09° which deviates slightly from 120° (characteristic of sp^2 hybridization), but it is far away from 109.47° (characteristic of sp^3 hybridization). Thus C atoms in CAs_3 monolayer prefers sp^2 -like hybridization in which one s and two p orbitals ($2p_x$ and $2p_y$) combine to produce three hybridized orbitals which in turn make three covalentlike bonds (three valence electrons of C) with its three nearest neighbor As atoms (one electron each). The fourth electron will be in the unhybridized p_z orbital. However, it is important to note that since the bond angles centered around C atoms is not perfectly 120° , the hybridization cannot purely sp^2 . Thus it is expected that there will be a small mixing between the $2p_z$ and sp^2 hybridized orbitals. Our analysis of partial DOS indicates that the valence and conduction bands around the E_F are due to these mixed orbitals.

In order to verify this fact, we have plotted the Kohn-Sham (KS) states corresponding to highest occupied valence and lowest unoccupied conduction states in Fig. 6. It is to be noted that these two states are degenerate and occur at the high-symmetry K point in the Brillouin zone. The plots of KS states clearly show the presence of two-lobed (dumbbell-like shape) of $2p_z$ around C atoms. We can also see a contribution from orbitals of As atoms due to the above mentioned mixing between p_z and sp^2 hybridized orbitals. This suggests the existence of a strong correlation between the linear dispersion (Dirac cone) around the E_F and sp^2 -like (which includes $2p_z$) orbital of C atom. This observation is similar to the one found in buckled silicene and germanene monolayers where

the $3p_z$ and $4p_z$ orbitals respectively contribute strongly to the states which form Dirac cones in these two systems. It is important to note here that the bond angle between the Si atoms in silicene [10] is 116.08° which is quite close to the angle As-C-As observed in the present case. This indicates the similarity between the CAs_3 monolayer and silicene, in buckled configuration, where the hybridization is a mixture of sp^2 and $3p_z$ orbitals of Si atom. Further, in case of silicene, the overlap between the $3p_z$ orbitals is weak due to the large internuclear distance Si-Si (as compared to C-C in graphene).

We wish to note here that the existing results in the literature on various two-dimensional monolayers such as graphene, silicene, germanene, arsenene, aluminene, etc. suggest that the crystal symmetry of 2D system strongly influences the nature of dispersion around the Fermi level. In case of graphene and aluminene [6], the hexagonal symmetry with pure sp^2 hybridization leads to linear dispersion in the electronic band structures in these two systems. The main difference is that the Dirac point (crossing of linear dispersions) lies exactly at the Fermi level in the former but it lies above the Fermi level in the latter. Whereas the other group IV monolayers such as silicene and germanene possess trigonal crystal symmetry instead of hexagonal due to the presence of buckling in the geometry. Thus the hybridization is not purely sp^2 but a mixture of sp^2 and sp^3 . In spite of this, these two systems show linear dispersions around the Fermi level. On the other hand, the group V based monolayers, namely, phosphorene and arsenene, favor orthorhombic crystal systems and they do not show linear dispersion, but they are semiconductors with parabolic dispersions. However, it has been reported that under influence of strain, it is also possible to produce the linear dispersion in puckered arsenene [22]. Interestingly, the linear dispersion appears when the strain causes the local geometric arrangement around As atom contains threefold symmetry. Thus we wish to say that the symmetry plays an important role in determining the nature of the states around the Fermi level. It is well known that the symmetry is closely connected with the hybridization between the orbitals of the constituent atoms. In the present work, for CAs_3 monolayer in buckled configuration, we observe that there is a correlation between the appearance of linear dispersion and hybridization of orbitals of C atoms. Unlike As atom, the geometric arrangement around C atoms has threefold rotational symmetry. As mentioned in the previous section, the bond angle centered around C atoms (116.09°) is close to that of sp^2 hybridization rather than that of sp^3 hybridization. In order to study the influence of the hybridization on the linear dispersion and also to probe the possibility of tuning the Dirac point, we have also carried out the investigation of effect of mechanical strain on the electronic structure of CAs_3 monolayer in buckled configuration. The results again suggest the presence of correlation between the sp^2 -like hybridization of orbital of C and the linear dispersion. The details will be discussed in the next section.

C. Effect of mechanical strain on properties of buckled configuration

To study the influence of mechanical strain, we have performed the electronic structure calculations of CAs_3

monolayer under biaxial, both compressive and tensile, strains. The effect of strain has been simulated by freezing the lattice constant a to a particular value other than the equilibrium lattice constant a_0 (6.778 Å). With this fixed value of lattice constant, the fractional coordinates of all the atoms in the unit cell have been optimized with the convergence criteria mentioned in Sec. II. The percentage of strain is calculated by using the expression $[(a - a_0)/a_0] \times 100\%$. The positive and negative values of strain represent the tensile and compressive strains, respectively. In the present study, we have varied the values of strains from -20% to 20% in steps of 2% .

1. Geometry and energetics

Our results for the binding energy, geometrical parameters (buckling lengths, bond angles) and electronic band structures of CAs_3 monolayer with mechanical strains are summarized in Figs. 7 and 8. Variation of binding energy with strain shows a parabolic curve with a stable minima at the equilibrium lattice constant [see Fig. 7(a)]. However, when the magnitude of the strain is large, there is a clear deviation from the parabolic trend. Further, it is observed that both the buckling lengths h_1 and h_2 change monotonically with the strain, though the rate of variation in h_2 is larger as compared to that in h_1 . When the tensile strain reaches 18% , the values of these two buckling lengths decrease sharply and become nearly zero (~ 0.01 Å) at 20% of strain. Furthermore, the two bond angles, namely, As-As-As and C-As-As, also show a clear monotonic rise with increasing the tensile strain. In case of the angle As-C-As, we observe that the slope of the variation is very small. In this case, angle is increased from 116.09° to 116.40° when we go from equilibrium structure to 16% of tensile strain. All the three angles suddenly decrease around 18% of strain and reach almost 120° at 20% of strain. This indicates that the buckled configuration is reduced to the planar configuration. For the sake of comparison, the data point corresponding to binding energy of the planar configuration is included (black colored open symbol) in Fig. 7(a). This point falls closely to that of the buckled configuration with 18% of strain. It is to be noted here that the value of lattice constant for the planar configuration (7.964 Å) is equal to that of buckled configuration with 17.5% of tensile strain. On the other hand, for compressive strains, the value of h_1 increases slowly until there is a sharp increase at -14% of strain. Similarly, the value of h_2 also undergoes a drastic rise at -18% of strain. Further, we also observe abrupt changes in the values of three angles beyond -14% of compressive strains. These results clearly indicate that the bonds between As atoms are broken and the geometry of atoms in the unit cell turns as two molecular units of CAs_3 [see insert in Fig. 7(a) for geometry with strain of -18%].

2. Electronic structure

In Fig. 8, we plot the electronic band structure of buckled CAs_3 monolayer with different values of mechanical strain, ranging from -20% to $+20\%$. Many important modifications in the electronic band structures due to the application of mechanical strain on the system have been observed. Firstly, it is clearly seen that the linear dispersion disappears for compressive strain beyond -12% . The presence of the linear

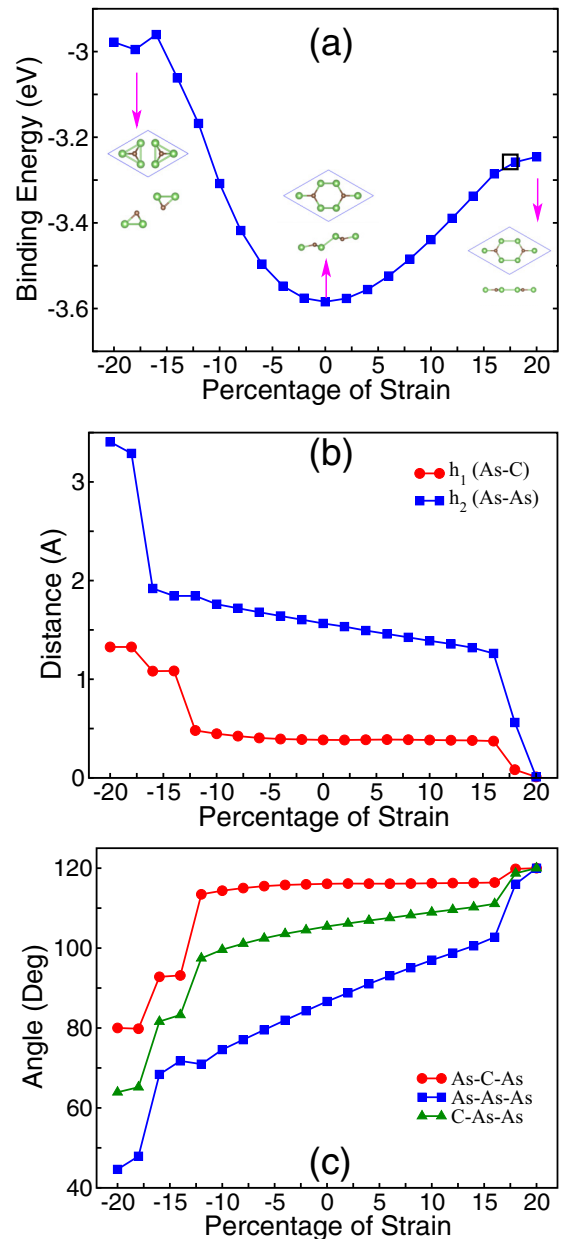


FIG. 7. Variation of (a) binding energy, (b) distances (h_1 , h_2), and (c) angles for CAs_3 monolayer with the biaxial strain. The open square represents the binding energy of the planar configuration.

dispersion (and hence Dirac cone) around the high-symmetry K point is clearly observed for an applied strain ranging from -12% to $+20\%$. However, the Dirac point may not lie exactly at the E_F . Reason for the disappearance of linear dispersion beyond -12% can be traced back to the modification in the geometry and hence the hybridization. When the compressive strain change from -12% to -14% , there are drastic changes in the values of bond angles (As-C-As, C-As-As) and buckling length (h_1 , which is a vertical length between C and As atoms). This clearly indicates that major changes occur in the geometrical arrangements around C atoms. These changes will strongly influence the hybridization and hence the electronic properties of the system. For instance, the bond angle As-C-As is changed from

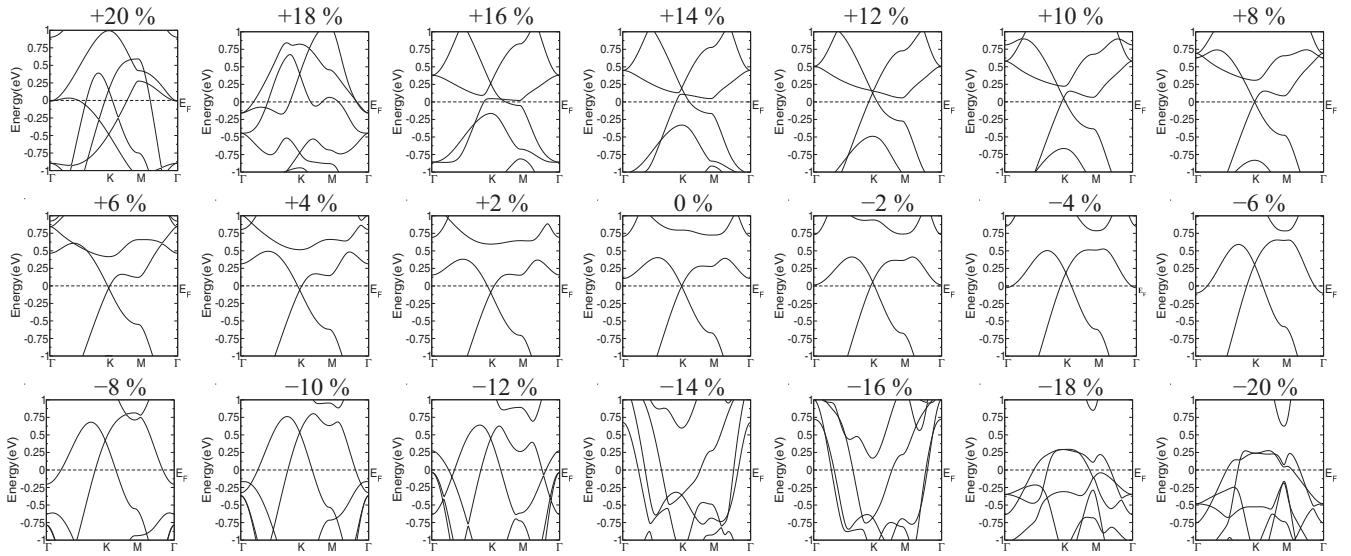


FIG. 8. Variation of electronic band structure of CAS_3 monolayer with biaxial strains from -20% to $+20\%$.

113.45° to 93.15° when we go from -12% to -14% of strain. Due to this, the overlap of $2p_z$ orbital of C with those of sp^2 orbitals becomes so large that the $2p_z$ orbital almost loses its individuality as an unhybridized orbital. In this case, the mixing leads to a situation similar to sp^3 hybridization. Subsequently, the feature of linear dispersion disappears in the electronic band structure. These results indicate that the presence of linear dispersion in the electronic band structure of CAS_3 monolayer in buckled configuration can be correlated with the sp^2 -like hybridization of orbitals of C atom. Whenever the hybridization of orbitals of C atom deviates strongly from sp^2 due to mechanical strain, the linear dispersion disappears from the electronic band structure.

As we have discussed in the previous section, the Dirac point lies exactly at the E_F for CAS_3 monolayer without any strain. When CAS_3 monolayer is subjected to compressive strain ranging from 0 to -12% , it is observed that the position of the Dirac point is systematically pushed upward and it reaches maximum energy of 0.47 eV above the E_F . Thus the mechanical strain can be useful tool to tune the position of the Dirac point. It is also important to note that the parabolic-like dispersion, which exists around the Γ at 105 meV above the E_F in the unstrained system, has also been pushed below the E_F due to the compressive strain. It is getting occupied by the electron at -4% of strain. Similarly, we also note that few occupied parabolic-like bands (which were much below -1.0 eV) around the Γ points have also been pushed upward towards the E_F due to the compressive strain. In case of tensile strain, we observe that the position of the Dirac point fluctuates around the E_F for small amount of strain of about less than 10% and it moves upward for a strain larger than this amount. It is also observed that the conduction bands which lie above 0.7 eV in the unstrained monolayer start moving towards the E_F due to the application of tensile strain. Importantly, there are no other dispersion curves which cross the E_F or come closer to the Dirac point for the tensile strain range from 0 to 10%. Thus, for this range of the tensile strain, the transport properties of the system is mainly characterized by the massless Dirac Fermions. For 12% of strain, we ob-

serve that one of the high lying conduction bands comes close to the Dirac point and it crosses the Dirac point for higher strain. Hence, this band may lie exactly at the Dirac point for a value of strain little above 12%. In this situation, these three bands touching at a point may lead to the appearance of triplet Fermions in the system which is similar to one observed in β_{12} borophene [64]. For strain beyond 16%, few conduction bands cross the E_F which make both Dirac- and Schrodinger-like Fermions to contribute to the electronic properties of CAS_3 monolayer. Overall, we find that the mechanical strain can be an useful tool to modify the properties of CAS_3 monolayer.

IV. CONCLUSION

Using density functional theory based electronic structure calculations, we have predicted the energy and dynamical stabilities of CAS_3 monolayer in buckled and puckered configurations. However, the planar configuration is found to be dynamically unstable. The buckled monolayer is found to be energetically most stable configuration and it is followed by the puckered configuration with difference in binding energy of 15 meV/atom. Our results of electronic structure calculations suggest that puckered CAS_3 is a metal since it contains finite density of state at the Fermi level. We found that the geometrical arrangement in the buckled configuration is slightly different from those observed for silicene and germanene. We have observed from the results of electronic structure calculations that CAS_3 monolayer is a semimetal. In addition, our results indicate that the electronic band structure of this monolayer possesses a linear dispersion (2D band structure, E versus k) at the Fermi level around the high symmetric K point of the reciprocal lattice. The presence of a Dirac cone around the K point at the E_F is also confirmed in the three-dimensional electronic band structure [E versus (k_x, k_y)]. Thus the charge carriers in this system behave as massless Dirac fermion for low-energy excitation (< 105 meV). This suggests that the properties of CAS_3 monolayer are similar to those of graphene, silicene and germanene. Our detailed analysis

of partial density of state indicates that the $2p_z$ orbital of C atoms contributes significantly to the states which form the linear dispersion and hence the Dirac cone around the Fermi level. This result clearly suggests the existence of a strong correlation between the linear dispersion (Dirac cone) and sp^2 -like hybridization of the orbitals of C atom. We have also studied the effect of mechanical strain on the properties of CAs_3 monolayer. For a tensile strain beyond 18%, the buckled configuration is reduced to the planar configuration. There are drastic changes in the geometrical environment around C atom in the unit cell when the compressive strain increased beyond -12% and hence the hybridization between the orbitals of C atoms changes. This leads to the disappearance of linear dispersion in the electronic band structure. We also have observed a systematic upward shift in the position of the Dirac

point due to the compressive strain which can be an useful tool to the modify the properties of CAs_3 monolayer. Finally, it is important to note that this monolayer system belongs to the class of *Dirac materials* and hence, like graphene, several properties of this system at low energy excitation are governed by the Dirac-like Hamiltonian.

ACKNOWLEDGMENTS

The author thanks A. Chakrabarti for critical reading of the manuscript and fruitful discussions. The author also thanks A. Banerjee for the discussions. P. A. Naik is thanked for constant support and encouragement. Scientific Computing Group, Computer Division, RRCAT is thanked for providing help and support in running the codes.

-
- [1] A. H. Castro Neto, F. Guinea, N. M. R. Peres, K. S. Novoselov, and A. K. Geim, *Rev. Mod. Phys.* **81**, 109 (2009) and references therein.
- [2] M. I. Katsnelson, *Graphene: Carbon in Two Dimensions* (Cambridge University Press, Cambridge, 2012).
- [3] J. Kunstmann and A. Quandt, *Phys. Rev. B* **74**, 035413 (2006).
- [4] H. Tang and S. Ismail-Beigi, *Phys. Rev. Lett.* **99**, 115501 (2007).
- [5] X. Wu, J. Dai, Y. Zhao, Z. Zhuo, J. Yang, and X. C. Zeng, *ACS Nano* **6**, 7443 (2012).
- [6] C. Kamal, A. Chakrabarti, and M. Ezawa, *New J. Phys.* **17**, 083014 (2015).
- [7] K. Takeda and K. Shiraishi, *Phys. Rev. B* **50**, 14916 (1994).
- [8] G. G. Guzmán-Verri and L. C. Lew Yan Voon, *Phys. Rev. B* **76**, 075131 (2007).
- [9] S. Cahangirov, M. Topsakal, E. Aktürk, H. Şahin, and S. Ciraci, *Phys. Rev. Lett.* **102**, 236804 (2009).
- [10] C. Kamal, A. Chakrabarti, A. Banerjee, and S. K. Deb, *J. Phys. Cond. Mat.* **25**, 085508 (2013).
- [11] C. Kamal, A. Banerjee, and A. Chakrabarti, *Graphene Science Handbook: Size-Dependent Properties*, edited by M Aliofk-hazraei *et al.* (CRC Press, 2016), Chap. 15, pp. 221–234 and references therein.
- [12] C. Kamal, A. Chakrabarti, and A. Banerjee, *Phys. Lett. A* **378**, 1162 (2014).
- [13] C. C. Liu, H. Jiang, and Y. Yao, *Phys. Rev. B* **84**, 195430 (2011).
- [14] J. C. Garcia, D. B. de Lima, L. V. C. Assali, and J. F. Justo, *J. Phys. Chem. C* **115**, 13242 (2011).
- [15] A. Acun, L. Zhang, P. Bampoulis, M. Farmanbar, A. van Houselt, A. N. Rudenko, M. Lingenfelder, G. Brocks, B. Poelsema, M. I. Katsnelson, and H. J. W. Zandvliet, *J. Phys. Cond. Mat.* **27**, 443002 (2015).
- [16] B. van den Broek, M. Houssa, E. Scalise, G. Pourtois, V. V. Afanasev, and A. Stesmans, *2D Materials* **1**, 021004 (2014).
- [17] P. Rivero, J.-A. Yan, V. M. García-Suárez, J. Ferrer, and S. Barraza-Lopez, *Phys. Rev. B* **90**, 241408(R) (2014).
- [18] V. O. Özçelik, O. Ü. Aktürk, E. Durgun, and S. Ciraci, *Phys. Rev. B* **92**, 125420 (2015).
- [19] J. Qiao, X. Kong, Z. X. Hu, F. Yang, and W. Ji, *Nat. Commun.* **5**, 4475 (2014).
- [20] V. Tran, R. Soklaski, Y. Liang, and L. Yang, *Phys. Rev. B* **89**, 235319 (2014).
- [21] A. N. Rudenko and M. I. Katsnelson, *Phys. Rev. B* **89**, 201408(R) (2014).
- [22] C. Kamal and M. Ezawa, *Phys. Rev. B* **91**, 085423 (2015).
- [23] S. Zhang, Z. Yan, Y. Li, Z. Chen, and H. Zeng, *Angew. Chem. Int. Ed.* **54**, 3112 (2015).
- [24] E. Aktürk, O. Ü. Aktürk, and S. Ciraci, *Phys. Rev. B* **94**, 014115 (2016).
- [25] A. J. Mannix, X. F. Zhou, B. Kiraly, J. D. Wood, D. Alducin, B. D. Myers, X. Liu, B. L. Fisher, U. Santiago, J. R. Guest, M. J. Yacaman, A. Ponce, A. R. Oganov, M. C. Hersam, and N. P. Guisinger, *Science* **350**, 1513 (2015).
- [26] B. Feng, J. Zhang, Q. Zhong, W. Li, S. Li, H. Li, P. Cheng, S. Meng, L. Chen, and K. Wu, *Nat. Chem.* **8**, 563 (2016).
- [27] B. Lalmi, H. Oughaddou, H. Enriquez, A. Kara, S. Vizzini, B. Ealet, and B. Aufray, *Appl. Phys. Lett.* **97**, 223109 (2010).
- [28] P. Vogt, P. D. Padova, C. Quaresima, J. Avila, E. Frantzeskakis, M. C. Asensio, A. Resta, B. Ealet, and G. L. Lay, *Phys. Rev. Lett.* **108**, 155501 (2012).
- [29] A. Fleurence, R. Friedlein, T. Ozaki, H. Kawai, Y. Wang, and Y. Yamada-Takamura, *Phys. Rev. Lett.* **108**, 245501 (2012).
- [30] L. Tao, E. Cinquanta, D. Chiappe, C. Grazianetti, M. Fanciulli, M. Dubey, A. Molle, and D. Akinwande, *Nat. Nanotechnol.* **10**, 227 (2015).
- [31] M. E. Davila, L. Xian, S. Cahangirov, A. Rubio, and G. L. Lay, *New J. Phys.* **16**, 095002 (2014).
- [32] M. Derivaz, D. Dentel, R. Stephan, M-C. Hanf, A. Mehdaoui, P. Sonnet, and C. Pirri, *Nano Lett.* **15**, 2510 (2015).
- [33] M. E. Davila and G. L. Lay, *Sci. Rep.* **6**, 20714 (2016).
- [34] F. F. Zhu, W. J. Chen, Y. Xu, C.-L. Gao, D.-D. Guan, C.-H. Liu, D. Qian, S.-C. Zhang, and J.-F. Jia, *Nat. Mater.* **14**, 1020 (2015).
- [35] S. Saxena, R. P. Chaudhary, and S. Shukla, *Sci. Rep.* **6**, 31073 (2016).
- [36] J. Gao, G. Zhang, and Y. W. Zhang, *Sci. Rep.* **6**, 29107 (2016).
- [37] L. Li, Y. Yu, G. J. Ye, Q. Ge, X. Ou, H. Wu, D. Feng, X. H. Chen, and Y. Zhang, *Nat. Nanotech.* **9**, 372 (2014).
- [38] A. Castellanos-Gomez, L. Vicarelli, E. Prada, J. O. Island, K. L. Narasimha-Acharya, S. I. Blanter, D. J. Groenendijk, M.

- Buscema, G. A. Steele, J. V. Alvarez, H. W. Zandbergen, J. J. Palacios, and H. S. J. van der Zant, *2D Mater.* **1**, 025001 (2014).
- [39] H. S. Tsai, S. W. Wang, C. H. Hsiao, C. W. Chen, H. Ouyang, Y. L. Chueh, H. C. Kuo, and J. H. Liang, *Chem. Mater.* **28**, 425 (2016).
- [40] M. Pumera and Z. Sofer, *Adv. Mater.* **29**, 1605299 (2017).
- [41] F. Reis, G. Li, L. Dudy, M. Bauernfeind, S. Glass, W. Hanke, R. Thomale, J. Schäfer, and R. Claessen, *Science* **357**, 287 (2017).
- [42] Z. Ni, Q. Liu, K. Tang, J. Zheng, J. Zhou, R. Qin, Z. Gao, D. Yu, and J. Lu, *Nano Lett.* **12**, 113 (2012).
- [43] N. D. Drummond, V. Zólyomi, and V. I. Falko, *Phys. Rev. B* **85**, 075423 (2012).
- [44] M. Ezawa, *New J. Phys.* **14**, 033003 (2012).
- [45] C. Kamal, [arXiv:1202.2636v1](https://arxiv.org/abs/1202.2636v1) [cond-mat.mes-hall].
- [46] T. O. Wehling, A. M. Black-Schaffer, and A. V. Balatsky, *Adv. Phys.* **63**, 1 (2014).
- [47] H. Sahin, S. Cahangirov, M. Topsakal, E. Bekaroglu, E. Akturk, R. T. Senger, and S. Ciraci, *Phys. Rev. B* **80**, 155453 (2009).
- [48] C. Kamal, A. Chakrabarti, and M. Ezawa, *Phys. Rev. B* **93**, 125428 (2016).
- [49] Y. Jing, Y. Ma, Y. Li, and T. Heine, *Nano Lett.* **17**, 1833 (2017).
- [50] B. Ghosh, S. Puri, A. Agarwal, and S. Bhowmick, *J. Phys. Chem. C* **122**, 18185 (2018).
- [51] L.-P. Feng, A. Li, P.-C. Wang, and Z.-T. Liu, *J. Phys. Chem. C* **122**, 24359 (2018).
- [52] L. T. Hoa, H. N. Tien, V. H. Luan, J. S. Chung, and S. H. Hur, *Sens. Actuators, B* **185**, 701 (2013); Z. L. Wang, *Appl. Phys. A* **88**, 7 (2007); P. K. Kanna, D. J. Late, H. Morgan, and C. S. Rout, *Nanoscale* **7**, 13293 (2015).
- [53] G. Kresse and J. Furthmüller, *Phys. Rev. B* **54**, 11169 (1996); G. Kresse and D. Joubert, *ibid.* **59**, 1758 (1999); VASP 5.2 programme package used here is fully integrated in the MedeA platform (Materials Design, Inc.) with a graphical user interface for the computation of the properties.
- [54] P. E. Blöchl, *Phys. Rev. B* **50**, 17953 (1994).
- [55] P. Hohenberg and W. Kohn, *Phys. Rev.* **136**, B864 (1964); W. Kohn and L. J. Sham, *ibid.* **140**, A1133 (1965).
- [56] J. P. Perdew, K. Burke, and M. Ernzerhof, *Phys. Rev. Lett.* **77**, 3865 (1996).
- [57] K. Momma and F. Izumi, *J. Appl. Crystallogr.* **41**, 653 (2008); <http://jp-minerals.org/vesta/en>.
- [58] A. Togo, Phonopy, <http://phonopy.sourceforge.net>.
- [59] S. Maintz, V. L. Deringer, A. L. Tchougreeff, and R. Dronskowski, *J. Comput. Chem.* **37**, 1030 (2016).
- [60] Y. Aierken, D. Çakir, C. Sevik, and F. M. Peeters, *Phys. Rev. B* **92**, 081408(R) (2015).
- [61] O. Ü. Aktürk, V. O. Özçelik, and S. Ciraci, *Phys. Rev. B* **91**, 235446 (2015).
- [62] V. O. Özçelik, E. Durgun, and S. Ciraci, *J. Phys. Chem. Lett.* **5**, 2694 (2014).
- [63] N. J. Roome and D. Carey, *ACS Appl. Mater. Int.* **6**, 7743 (2014).
- [64] M. Ezawa, *Phys. Rev. B* **96**, 035425 (2017).